Published in final edited form as:
ACS Chem Biol. 2011 May 20; 6(5): 413–418. doi:10.1021/cb200004k.

Binding and pK_a Modulation of a Polycyclic Substrate Analog in a Type II Polyketide Acyl Carrier Protein

Robert W. Haushalter, **Fabian V. Filipp**, **Kwang-seuk Ko**, **Ricky Yu**, **Stanley J. Opella**, and **Michael D. Burkart**
Department of Chemistry and Biochemistry, University of California San Diego, 9500 Gilman Drive, La Jolla, CA 92037-0358

Abstract

Type II polyketide synthases are biosynthetic enzymatic pathways responsible for the production of complex aromatic natural products with important biological activities. In these systems, biosynthetic intermediates are covalently bound to a small acyl carrier protein that associates with the synthase enzymes and delivers the bound intermediate to each active site. In the closely related fatty acid synthases of bacteria and plants, the acyl carrier protein acts to sequester and protect attached intermediates within its helices. Here we investigate the type II polyketide synthase acyl carrier protein from the actinorhodin biosynthetic pathway and demonstrate its ability to internalize the tricyclic, polar molecule emodic acid. Elucidating the interaction of acyl carrier proteins with bound analogs resembling late-stage intermediates in the actinorhodin pathway could prove valuable in efforts to engineer these systems towards rational design and biosynthesis of novel compounds.

INTRODUCTION

Type II polyketide synthases (PKSs) catalyze the iterative condensation of malonate precursors into polycyclic natural products of critical medicinal importance (1–4). Some notable examples include the widely prescribed tetracycline antibiotics and the anti-cancer therapeutic doxorubicin. The central component of these pathways is an acyl carrier protein (ACP) that shuttles thioester-bound intermediates between catalytic domains while attached to the terminus of a 4’-phosphopantetheine (4’PP) prosthetic group. In type II fatty acid synthases (FAS), the ACP has been shown to envelop the growing polymer, serving to protect the thioester bond from hydrolysis (5–8). This internalization of intermediates could also be advantageous in type II PKS pathways. Both pathways share the sensitive thioester linkage, and PKS intermediates are highly reactive and prone to aberrant cyclization (1).

The biosynthesis of actinorhodin in *Streptomyces coelicolor* A3(2) is outlined in Fig. 1a (9–13). In contrast to FAS systems, the β-ketone produced after each elongation step remains intact for multiple rounds of chain extension, yielding the *acyl*-actACP species **3** with an octaketide intermediate bound via 4’PP. Controlled cyclization of this acyl chain and release of the tricyclic polyketide dihydrokalafungin **4** is mediated by ketoreductase (KR) and aromatization / cyclization (ARO/CYC) domains. In the absence of KR and ARO/CYC, the acyl chain of **3** will spontaneously cyclize to afford a variety of aldol and claisen condensation products (11,14). Because of the synthetic challenges in producing

Correspondence to: Michael D. Burkart.

Supporting Information Available: This material is free *via* the Internet.

intermediate **3** *in vitro*, including its inherent instability, the interactions between the acyl chain and actACP in this intermediate remain uncharacterized.

Although substrate sequestration of intermediates in type II FAS is well documented (5–8), investigations into this phenomenon in PKS ACPs remain poorly understood. Evans et al. (15) reported the solution NMR structures of several *acyl*-actACP species, including several saturated acyl chains and two short-chain polyketide intermediates, all of which were attached via thioether linkage to *holo*-actACP. The saturated fatty acyl groups were bound within a cleft between helix II and helix III of actACP in a manner analogous to FAS ACPs. In contrast, the short-chain polyketide intermediates interacted with the protein to a lesser extent and induced partial opening of the actACP binding cavity. One of these *acyl*-ACP species, *3,5-dioxohexyl*-actACP, was shown to exist in two conformations. In the minor conformer, association of the acyl chain with actACP was observed, as evidenced by chemical shift differences between the 2D NMR spectra of this species and *holo*-actACP, as well as six NOE signals (15).

In our current study, we have sought to further characterize interactions between actACP and bound acyl groups by appending a cyclic, polar substrate analog that resembles extended polyketide intermediates. To this end, we employed chemoenzymatic methods (16–18) to append the tricyclic anthraquinone emodic acid to actACP at the terminus of a 4'-phosphopantetheine isostere (Fig. 1b). Although emodic acid itself is not a physiological intermediate in the actinorhodin pathway, the tricyclic portion of the tethered emodic-pantetheinamide ligand **5** resembles cyclized product **4** both sterically and in polarity and the parent compound emodin has been shown to bind in the actKR active site with low μM affinity (11). Additionally, this compound deprotonates near neutral pH, resulting in a color change from yellow to pink, which facilitates colorimetric observation of the molecule's protonation state. Our results confirm that the emodic acid group is bound in the cleft between helix II and helix III in a similar fashion to the fatty acyl chains studied previously.

RESULTS

Comparison of *holo*-actACP and *emodic*-actACP on conformationally-sensitive urea PAGE (19,20) revealed that loading of **5** retards the migration of the protein (Fig. S1). Previous structural studies of actACP have indicated that the protein is capable of expanding its internal binding cavity, resulting in the opening of an unoccupied volume deep within actACP (15). Therefore, these results suggest that it could accommodate cyclized substituents than are bulkier than the linear acyl chains investigated. Decreased urea PAGE mobility of *emodic*-actACP **6** compared to *holo*-actACP **2** indicates an expansion of the hydrodynamic radius of the protein, consistent with internal binding of the bulky emodic acid group (19,20).

NMR spectroscopy has been the most successful technique to study ACPs at the molecular level given their intrinsically dynamic structures (21–24). In order to focus on the effects of the emodic acid moiety and not the 4'PP arm, the NMR spectra of *emodic*-actACP **6** and *holo*-actACP **2** compared. The two-dimensional ^{1}H-^{15}N heteronuclear single quantum correlation (HSQC) spectra of *emodic*-actACP **6** and *holo*-actACP **2** in solution are well resolved. Unlike previously studied *acyl*-actACPs with polar acyl groups (15), we observed a single conformation of *emodic*-actACP. The backbone amide resonances in the HSQC spectra were assigned using data from 3D HNCA and HNCACB spectra (Fig.S2). Comparison of the spectra reveals pronounced chemical shift differences in several resonances (Fig. 2a). These changes in chemical shift were quantified and plotted as a function of residue number (Fig. 2c). The largest chemical shift perturbations were observed for residues in helix II, helix III, and the residues just C-terminal to helix III, with additional

perturbations on helix IV, and the loop preceding helix II. The residues with the largest chemical shift perturbations are located near the binding site between helix II and helix III (15).

Additionally, we acquired HSQC spectra of *apo*- and *octanoyl*-actACP to compare the chemical shift perturbations in these previously studied species with that of *emodic*-actACP (Fig. S6–S8). The HSQC spectra of *apo*- and *holo*-actACP have been fully assigned and reported previously (25), however, in this study we acquired the spectra under significantly different buffer conditions. The differences between *apo*- and *holo*-actACP HSQC spectra are subtle, consistent with previous comparisons (25), as seen in Fig S6. Both *octanoyl*- and *emodic*-actACP species used in this study contain non-hydrolysable amide bond linkages in place of a thioester or thioether bond to connect the pantetheine to the acyl groups of the molecules. Therefore, the carbonyl group at position 1 of an alkyl chain such as octanoate remains intact, providing a more isosteric substrate mimic than the thioether-bound acyl chains investigated previously (15). While many of the same residues were affected in *octanoyl*- and *emodic*-actACP relative to *holo*-actACP, the HSQC spectra of these species differ significantly, suggesting that the actACP interactions with the polar cyclic analog differ from those with a general hydrophobic acyl chain (Fig. S7, S8).

To further validate the interaction between actACP and the bound emodic acid moiety, we acquired 2D $^{13}C/^{15}N$-*F*1*F*2-filtered and $^{13}C/^{15}N$-*F*2-filtered-NOE spectra of *emodic*-actACP. NOE spectra give information about the spatial distances between nuclei as a crosspeak in the 2D spectrum at the chemical shifts of two nuclei in close proximity. These filtered NOE experiments take advantage of the lack of isotope enrichment in the emodic-pantetheinamide prosthetic group, as signals from protons bound to ^{13}C or ^{15}N (protons from the protein) are selectively filtered out (26). In the *F*1*F*2-filtered experiment (Fig 3a), only intramolecular NOE signals (within the prosthetic group) are observed. In the *F*2-filtered experiment (Fig. 3b), both intramolecular and intermolecular NOE signals (those between the prosthetic group and the protein) are visible. Therefore, resonances in the *F*2-filtered spectrum that are absent from the *F*1*F*2-filtered spectrum represent contacts between the appended prosthetic group and actACP. We detected >12 such NOE contacts between the aromatic protons from the emodic acid and side chain protons in the protein. The multiple intramolecular NOEs suggest that the 4'-PP portion of the prosthetic group is in a folded conformation consistent with other ACP species in which the appended acyl chain is bound within the protein (15), and the multiple emodic acid-to-protein NOEs detected indicate that the molecule is in close association with the protein. In order to glean information about the localization of the emodic acid within the protein, we then sought to assign the protein side chain protons in contact with the emodic acid group that give rise to the crosspeaks in the aliphatic region. To assign the resonances in the protein, we acquired a 3D HC(CO)NH spectrum of *emodic*-actACP, which yields the chemical shifts of protein side chain protons (27). With this information, we were able to positively assign NOE signals between the emodic acid group and the side chains of Leu45 and Ala65 (Fig.3). These NOE contacts agree closely with the pattern of HSQC perturbations described above, further supporting the localization of the emodic acid group between helix II and helix III. Ongoing experiments will allow us to unambiguously assign all NOE signals and solve the 3D structure of *emodic*-actACP. One possible evolutionary strategy to inhibit premature cyclization of intermediates such as the acyl chain of **3** is to prevent or slow down deprotonation of elongated polyketides to enolate species. Because **5** and **6** display a distinct color change between protonated and deprotonated states, we investigated the effect of protein sequestration on the pK_a of ACP-bound emodic acid. When protonated, **5** and **6** show a maximum absorbance at λ = 442 nm (yellow), while the deprotonated forms absorb at λ = 504 nm (pink/red). The UV-vis absorbance spectrum of *holo*-actACP showed no absorbance in the visible region at any pH, assuring that any absorbance at 442 nm or 504

nm is due to the emodic acid group. The ratio of absorbance at these two wavelengths was measured as a function of pH for free emodic-pantetheinamide **5** and for *emodic*-actACP **6**. When appended to actACP, the pK_a of the emodic acid group increases from 6.7 to 7.4 (Fig. 5). This supports a hypothesis in which ACP prevents premature cyclization of type II PKS intermediates by sequestering them within its helical core, inhibiting deprotonation until the ACP can deliver the intermediate from the KS/CLF to the KR (Fig. 1a).

DISCUSSION

The sequestration of late stage intermediates in type II PKS ACPs could have implications for the manipulation and engineering of these enzymatic assembly lines. Such sequestration of intermediates most likely induces changes in the shape of the ACP that affect protein-protein interactions controlling the biosynthetic progression in these pathways. In a combinatorial biosynthetic study by Wohlert et al., swapping of CYC domains from two PKSs resulted in complete loss of CYC activity (28), suggesting that proper activity is dependent on ACP-CYC interactions. These protein-protein interactions could be modulated by changes in the structure of ACP induced by bound intermediates. Recently, structures of a FAS ACP were reported for each bound intermediate over a complete cycle of chain extension, and it was found that bound intermediates induce small changes in ACP structure that could affect association with FAS enzymes (29). Analogously, the structural changes induced by sequestration of fully extended substrates in type II PKS could increase affinity for downstream KR and ARO/CYC domains. Catalytic domains such as KR and ARO/CYC (Fig.1a) must induce the physical release of intermediates from the ACP core into the active site of the enzyme. This transfer of acyl chains from the ACP interior into the active sites of partner enzymes, or “switchblade” activity, is a requisite phenomenon in FAS ACPs, and computational studies aimed at characterizing this event have recently been performed (30). Sequestration of intermediates in type II PKS suggests a similar requirement for switchblade activity. An understanding of this currently uncharacterized trigger will be key to elucidating the processivity of these pathways. We have demonstrated the interaction of the tricyclic emodic acid group within the type II PKS actACP. This interaction is stronger than that of short-chain polyketide intermediates investigated previously, as reflected by a single, associative conformation, more pronounced chemical shift perturbations, and multiple emodic acid-to-protein NOE signals. Our initial assignments indicate that the cyclic portion of **5** is located between helix II and helix III with direct interaction to key residues in these helices. We have developed preparative techniques to append a wide variety of substrate mimics to ACPs with isosteric connectivity, greatly expanding our ability to study type II PKS ACP interactions with bound functional groups. The possible diversity of bound functionalities that can be appended to ACPs using these techniques is vast; therefore, these tools should prove useful in studies of other modular synthase carrier proteins, including type I PKS and non-ribosomal peptide synthetases.

EXPERIMENTAL

More detailed experimental procedures, including synthetic procedures for compounds **5** and **S6**, cloning and expression of actACP, introduction of the C17S mutation, loading of actACP with compounds **5** and **S6,** and NMR characterization are available in the Supplemental Information.

Synthesis of emodic-pantetheinamide and octanoyl-pantetheinamide

Acetate-protected emodic acid **S1** was prepared as described previously (31). This protected emodic acid was coupled to PMB-protected pantetheine-amine **S2** using PyBop, and this intermediate was deprotected to give emodic-pantetheinamide **5.**

Octanoyl-pantetheinamide was synthesized via PyBop coupling PMB-protected pantetheine-amine **S2** with octanoic acid in THF. Deprotection with HCl yielded the final product **S6**.

Cloning of actACP C17S

The gene encoding actACP was cloned from *S. coelicolor* genomic DNA and was inserted into a pET-28b expression vector as described previously (32). A C17S mutation was introduced via quickchange PCR because the native cysteine residue has been shown to form problematic disulfide bonds with the terminal thiol of the 4'phosphopantetheine prosthetic group *in vitro* (33), and the cysteine could interfere with our ability to separate recombinantly expressed *apo*- and *holo*-actACP using thiosepharose resin (described below).

Expression, Modification, and Purification of *apo-*, *holo-*, *octanoyl-*, and *emodic*-ACP

pET28-actACP (C17S) plasmid was transformed into BL21 (DE3) cells. Uniformly labeled $^{13}C/^{15}N$-actACP was expressed by culturing 1L of cells in M9 minimal media supplemented in 1g of ^{15}N-ammonium sulfate and 2g U-^{13}C-glucose. Expression was induced with 1mM IPTG at OD_{600} of 0.5 and the cells were incubated an additional 4 hours at 37°C. When expressed recombinantly in *E. coli*, actACP was purified and found to be largely (>90%) in the *apo*- form. In order to obtain pure *apo*-actACP, the mixture was passed over thiosepharose resin that covalently binds *holo*-actACP. Pure *apo*-actACP was eluted from the resin. To produce *holo*-actACP, the *apo-/holo*- mixture was incubated with CoA and the PPTase Sfp. *Emodic*-actACP was produced in one pot chemoenzymatically by converting emodic-pantetheinamide **5** to the CoA analog *in situ* using ATP and three of the *E. coli* CoA biosynthetic enzymes, followed by loading onto *apo*-actACP by Sfp (17). *Octanoyl*-actACP was produced by the similar means with **S6**.

Urea PAGE of ACP species

Loading of emodic-pantetheinamide was monitored by urea PAGE gels consisting of 2M urea, 0.375M Tris-HCl pH 8.8, 20% acrylamide, 0.1% ammonium persulfate, 0.1% TEMED.

HSQC Spectra Acquisition and Assignment

HSQC spectra of all four actACP species were acquired on a Varian 800 MHz spectrometer. HNCA and HNCACB spectra of *holo*- and *emodic*-actACP were acquired on a Varian 500 MHz or a Bruker 600 MHz spectrometer. The 3D spectra allowed for unambiguous assignment of all backbone amide NH groups for residues 4–85 except prolines 61 and 71. HSQC perturbations were quantified using the formula $((\Delta H)^2 + 0.2(\Delta N)^2)^{1/2}$ (34).

Isotopically Filtered NOE spectra

$^{13}C/^{15}N$-*F*1*F*2-filtered and $^{13}C/^{15}N$-*F*2-filtered-NOE spectra of *emodic*-actACP were acquired on a Bruker 600 MHz spectrometer. To assign NOE resonances from actACP side chains, we acquired a 3D HC(CO)NH spectrum of *emodic*-actACP at 600 MHz.

pH Titration of emodic-pantetheinamide and *emodic*-actACP

Both species were dissolved in phosphate buffered saline pH 5.5 and the pH was raised incrementally with additions of small volumes of 6M NaOH. The UV-vis absorption spectrum was acquired at each pH value. A shift in λ_{max} from 442nm to 504nm and a color change from yellow to pink is observed upon deprotonation of the emodic group.

Supplementary Material

Refer to Web version on PubMed Central for supplementary material.

Acknowledgments

We would like to thank Dr. Xuemei Huang and Dr. Anthony Mrse of the UCSD Biomolecular NMR facility for their assistance in acquiring NMR spectra, as well as Dr. Gabriel Cook, Dr. Fabio Casagrande and Yan Wang for their assistance in processing NMR data. Thanks to Mike Wuo for assistance in the synthesis of emodic-pantetheinamide. We would also like to thank Dr. James LaClair, Dr. Joris Beld, and Prof. Patricia Jennings for their insightful conversations and advice. This work was funded by NIH GM075797 and NIH GM086225.

References

1. Das A, Khosla C. Biosynthesis of aromatic polyketides in bacteria. Acc Chem Res. 2009; 42:631–639. [PubMed: 19292437]
2. Tsai SC, Ames BD. Structural enzymology of polyketide synthases. Methods Enzymol. 2009; 459:17–47. [PubMed: 19362634]
3. Hertweck C, Luzhetskyy A, Rebets Y, Bechthold A. Type II PKS: Gaining a deeper insight into enzymatic teamwork. Nat Prod Rep. 2007; 24:162–190. [PubMed: 17268612]
4. Katz L, Donadio S. Polyketide synthesis: prospects for hybrid antibiotics. Annu Rev Microbiol. 1993; 47 :875–912. [PubMed: 8257119]
5. Mercer AC, Burkart MD. The ubiquitous carrier protein--a window to metabolite biosynthesis. Nat Prod Rep. 2007; 24:750–773. [PubMed: 17653358]
6. Zornetzer GA, Fox BG, Markley JL. Solution structures of spinach acyl carrier protein with decanoate and stearate. Biochemistry. 2006; 45:5217–5227. [PubMed: 16618110]
7. Roujeinikova A, Baldock C, Simon WJ, Gilroy J, Baker PJ, Stuitje AR, Rice DW, Slabas AR, Rafferty JB. X-ray crystallographic studies on butyryl-ACP reveal flexibility of the structure around a putative acyl chain binding site. Structure. 2002; 10:825–835. [PubMed: 12057197]
8. Roujeinikova A, Simon WJ, Gilroy J, Rice DW, Rafferty JB, Slabas AR. Structural studies on fatty acyl-(acyl carrier protein) thioesters reveal a hydrophobic binding cavity that can expand to fit larger substrates. J Mol Biol. 2007; 365:135–145. [PubMed: 17059829]
9. Hopwood DA. Genetic contributions to understanding polyketide synthases. Chem Rev. 1997; 97:2465–2498. [PubMed: 11851466]
10. Bisang C, Long PF, Cortes J, Westcott J, Crosby J, Matharu AL, Cox RJ, Simpson TJ, Staunton J, Leadlay PF. A chain initiation factor common to both modular and aromatic polyketide synthases. Nature. 1999; 401:502–505. [PubMed: 10519556]
11. Korman TP, Tan YH, Wong J, Luo R, Tsai SC. Inhibition kinetics and emodin cocrystal structure of a type II polyketide ketoreductase. Biochemistry. 2008; 47:1837–1847. [PubMed: 18205400]
12. Malpartida F, Hopwood DA. Molecular cloning of the whole biosynthetic pathway of a streptomyces antibiotic and its expression in a heterologous host. Nature. 1984; 309:462–464. [PubMed: 6328317]
13. Dreier J, Shah AN, Khosla C. Kinetic analysis of the actinorhodin aromatic polyketide synthase. J Biol Chem. 1999; 274:25108–25112. [PubMed: 10455191]
14. Kalaitzis JA, Moore BS. Heterologous biosynthesis of truncated hexaketides derived from the actinorhodin polyketide synthase. J Nat Prod. 2004; 67:1419–1422. [PubMed: 15332868]
15. Evans SE, Williams C, Arthur CJ, Cox RJ, Crosby J, Crump MP, Simpson TJ. Probing the interactions of early polyketide intermediates with the actinorhodin ACP from S. coelicolor A3(2). J Mol Biol. 2009; 389:511–528. [PubMed: 19361520]
16. La Clair JJ, Foley TL, Schegg TR, Regan CM, Burkart MD. Manipulation of carrier proteins in antibiotic biosynthesis. Chem Biol. 2004; 11:195–201. [PubMed: 15123281]
17. Worthington AS, Burkart MD. One-pot chemo-enzymatic synthesis of reporter-modified proteins. Org Biomol Chem. 2006; 4:44–46. [PubMed: 16357994]

18. Haushalter RW, Worthington AS, Hur GH, Burkart MD. An orthogonal purification strategy for isolating crosslinked domains of modular synthases. Bioorg Med Chem Lett. 2008; 18:3039–3042. [PubMed: 18249538]
19. Cronan JE. Molecular properties of short chain acyl thioesters of acyl carrier protein. J Biol Chem. 1982; 257:5013–5017. [PubMed: 7040391]
20. Post-Beittenmiller D, Jaworksi JG, Ohlrogge JB. *In vivo* pools of free and acylated acyl carrier proteins in spinach. J Biol Chem. 1991; 266:1858–1865. [PubMed: 1988450]
21. Oswood MC, Kim Y, Ohlrogge JB, Prestegard JH. Structural homology of spinach acyl carrier protein and *Escherichia coli* acyl carrier protein based on NMR data. Proteins. 1997; 27:131–143. [PubMed: 9037718]
22. Crump MP, Crosby J, Dempsey CE, Parkinson JA, Murray M, Hopwood DA, Simpson TJ. Solution structure of the actinorhodin polyketide synthase acyl carrier protein from *Streptomyces coelicolor* A3(2). Biochemistry. 1997; 36:6000–6008. [PubMed: 9166770]
23. Xu GY, Tam A, Lin L, Hixon J, Fritz CC, Powers R. Solution structure of *B. subtilis* acyl carrier protein. Structure. 2001; 9:277–287. [PubMed: 11525165]
24. Li Q, Khosla C, Puglisi JD, Liu CW. Solution structure and backbone dynamics of the holo form of the Frenolicin acyl carrier protein. Biochemistry. 2003; 42:4648–4657. [PubMed: 12705828]
25. Evans SE, Williams C, Arthur CJ, Burston SG, Simpson TJ, Crosby J, Crump MP. An ACP structural switch: conformational differences between the apo and holo forms of the actinorhodin polyketide synthase acyl carrier protein. Chembiochem. 2008; 9:2424–2432. [PubMed: 18770515]
26. Peterson RD, Theimer CA, Wu HH, Feigon J. New applications of 2D filtered/edited NOESY for assignment and structure elucidation of RNA and RNA-protein complexes. J Biomol NMR. 2004; 28:59–67. [PubMed: 14739639]
27. Logan TM, Olejniczak ET, Xu RX, Fesik SW. Side chain and backbone assignments in isotopically labeled proteins from two heteronuclear triple resonance experiments. FEBS Lett. 1992; 314:413–418. [PubMed: 1281793]
28. Wohlert S, Wendt-Pienkowski E, Bao W, Hutchinson CR. Production of aromatic minimal polyketides by the daunorubicin polyketide synthase genes reveals the incompatibility of the heterologous DpsY and JadI cyclases. J Nat Prod. 2001; 64:1077–1080. [PubMed: 11520231]
29. Ploskon E, Arthur CJ, Kanari AL, Wattana-amorn P, Williams C, Crosby J, Simpson TJ, Willis CL, Crump MP. Recognition of intermediate functionality by acyl carrier protein over a complete cycle of fatty acid biosynthesis. Chem Biol. 2010; 17:776–785. [PubMed: 20659690]
30. Colizzi F, Recanatini M, Cavalli A. Mechanical features of *Plasmodium falciparum* acyl carrier protein in the delivery of substrates. J Chem Inf Model. 2008; 12:2289–2293. [PubMed: 19007113]
31. Fonge H, Jin L, Wang H, Ni Y, Bormans G, Verbruggen A. Bioorg Med Chem Lett. 2007; 17:4001–4005. [PubMed: 17507220]
32. Yasgar A, Foley TL, Jadhav A, Inglese J, Burkart MD, Simeonov A. A strategy to discover inhibitors of *Bacillus subtilis* surfactin-type phosphopantetheinyl transferase. Mol Biosyst. 2010; 6:365–375. [PubMed: 20094656]
33. Crosby J, Byrom KJ, Hitchman TS, Cox RJ, Crump MP, Findlow IS, Bibb MJ, Simpson TJ. Acylation of streptomyces type II polyketide synthase acyl carrier proteins. FEBS Lett. 1998; 433:132–138. [PubMed: 9738947]
34. Pellecchia M, Sebbel P, Hermanns U, Wuthrich K, Glockshuber R. Pilus chaperone FimC-adhesin FimH interactions mapped by TROSY-NMR. Nat Struct Biol. 1999; 6:336–339. [PubMed: 10201401]

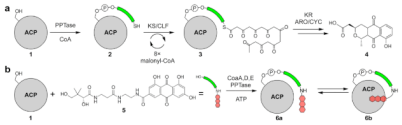

Figure 1.

Role of actACP in actinorhodin biosynthesis. (a) Actinorhodin PKS produces the dimeric tricyclic natural product actinorhodin. First, *apo*-actACP **1** is converted to *holo*-actACP **2** by installation of CoA-derived 4'-phosphopantetheine through the action of a PPTase. Condensation of 8 equivalents of ACP-bound malonate units by ketosynthase / chain length factor (KS/CLF) yield the *acyl*-ACP **3** with a bound octaketide intermediate. KR and ARO/CYC enzymes control the correct cyclization of this intermediate and dissociation from ACP to yield dihydrokalafungin **4**, which oxidizes and dimerizes to yield the final product actinorhodin. (b) Loading actACP with **5**. $^{13}C,^{15}N$-labeled *apo*-actACP is loaded with emodic-pantetheinamide analog **5** yielding *emodic*-actACP **6**. The emodic acid group is sequestered by actACP as depicted in **6b**.

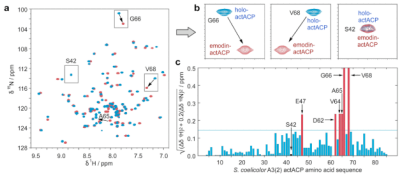

Figure 2.

Binding of a polyketide ligand by actACP causes strong and localized chemical shift perturbations in ^{1}H-^{15}N HSQC spectra. a) Overlayed HSQC spectra of *holo*-actACP (blue) and *emodic*-actACP (red). The shifts in residues Ala65, Gly66, and Val68 are highlighted. b) Close ups of residues Gly66, Val68, and Ser42. c) Chemical shift perturbations are measured between *holo*-actACP and *emodic*-actACP by ^{1}H, ^{15}N-correlation spectroscopy. Residues on helix II (Glu47), helix III (Asp62, Val64, Ala65), and the loop connecting helices III and IV (Gly66, Val68) show the strongest perturbations. Other significant perturbations are observed in the loop preceding helix II, the loop connecting helices II and III, and helix IV upon loading of the emodic acid group. The phosphopantetheine attachment site at serine 42 shows negligible difference between the two ACP species.

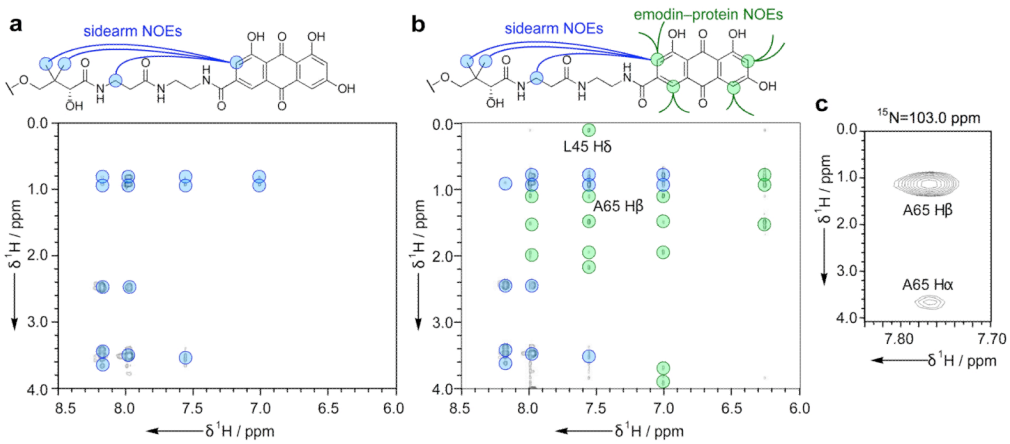

Figure 3.

a) $^{13}C/^{15}N$-*F*1*F*2-filtered NOE spectrum of *emodic*-actACP. This section of the spectrum focuses on NOE signals between aromatic protons on the emodic acid (δ^1H_x= 7.9, 7.55, 7.0, and 6.25 ppm) and protons in the aliphatic region (y-axis). Intramolecular NOEs between the emodic acid proton at 7.9 ppm and several protons in the 4'PP group were observed. b) $^{13}C/^{15}N$-*F*2-filtered-NOE spectra of *emodic*-actACP in the same region. The resonances observed in this spectrum that are absent in 3a are due to contacts between the emodic acid protons and the protein. We assigned resonances that correspond to side chain protons of residues Leu45 and Ala65. c) 2D slice of the 3D HC(CO)NH spectrum of *emodic*-actACP showing the side chain resonances of Ala65, which is resolved from other peaks. The Hβ protons of Ala65 are in close proximity to the emodic acid moiety, as shown by the crosspeaks in 3b.

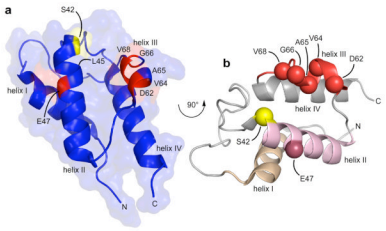

Figure 4.

Pymol structure of actACP (PDB: 2K0X) highlighting the residues in Fig. 2c that show the largest chemical shift perturbations between *holo*- and *emodic*-actACP. a) Residues that show the largest chemical shift perturbations are colored red. Leu45 is also indicated as we observed an NOE contact between the emodic acid and the side chain of this residue. b) Rotated view of actACP that with heavily perturbed residues indicated with spheres on the ribbon structure. The residues indicated surround a binding cleft located between helix II and helix III.

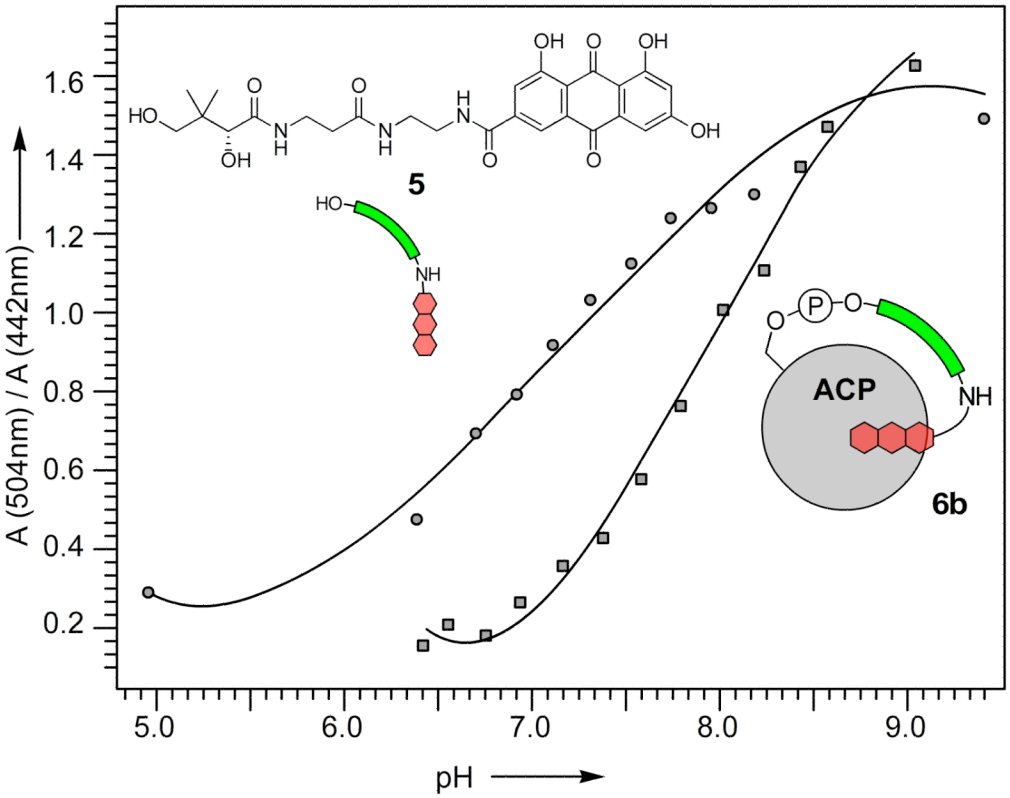

Figure 5.

pK_a profiles for emodic-pantetheinamide **5** (circles) and *emodic*-actACP **6** (squares). The ratio of absorbance values at 504nm (deprotonated) and 442nm (protonated) were measured at multiple pH values. The pK_a of the *emodic*-actACP is elevated compared to the free small molecule **5**.